Zhang, S. Y., Zhu, M., Li, Y., Jiang, J. Z., Ficca, R., Czechowicz, M., Neilson, R., Neild, S. A., & Herrmann, G. (2019). Ride comfort enhancement for passenger vehicles using the structure-immittance approach. *Vehicle System Dynamics: International Journal of Vehicle Mechanics and Mobility*. https://doi.org/10.1080/00423114.2019.1694158

ARTICLE TEMPLATE

Ride comfort enhancement for passenger vehicles using the structure-immittance approach

S.Y. Zhang[a,b], M. Zhu[a,b], Y. Li[a,b], J.Z. Jiang[a,b], R. Ficca[c], M. Czechowicz[c], R. Neilson[c], S.A. Neild[a,b] and G. Herrmann[a,b]

[a] Vibration Suppression Research Unit, Dynamics and Control Group, University of Bristol, Bristol, UK;
[b] Department of Mechanical Engineering, University of Bristol, Bristol, UK;
[c] Jaguar Land Rover, Viscount Center C, Milburn Hill Rd, Coventry, UK.
Word Count: 6872 (*approx*)

ARTICLE HISTORY
Compiled December 11, 2018

ABSTRACT
This paper investigates the ride comfort enhancement potential for passenger vehicles by employing inerter-spring-damping suspension struts. The inerter has been used on Formula 1 racing cars and several beneficial devices incorporating inerters have also been identified for ride comfort enhancement. However, previous investigations either were limited to simple network configurations with moderate performance improvement, or resulted in complicated configurations with a large number of elements which are impractical for real-life applications. In addition, some important practical performance constraints have not been taken into consideration, such as high-frequency dynamic stiffness which influences the NVH performance, and frequency content consideration of the sprung mass acceleration which more directly relates to passenger perception. In this paper, a quarter-car model including top mount is studied, with the performance of a conventional suspension strut presented as baseline. The structure-immittance approach, which can cover all networks with pre-determined numbers of each element type is adopted for identifying the optimal suspension configurations. Several configurations with up to a 13.3% performance improvement are identified with other practical performance indices to be no worse than the baseline. The suspension configurations proposed in previous works are also considered for a sake of comparison, demonstrating significant advantages of the structure-immittance approach. Subsequently, a sensitivity analysis against the sprung and unsprung mass changes is carried out, which represents cargo and tyre weight variations, respectively. Time domain response and other reality checks are then conducted for the out-performing configurations, which reconfirm the ride comfort enhancement and ensure no unexpected behaviour occurs.

KEYWORDS
inerter; structure-immittance approach; secondary ride comfort; high-frequency dynamic stiffness; tyre load; suspension travel

1. Introduction

When a vehicle travels on the road, it is always subjected to excitation from road irregularities, braking forces, acceleration forces, and inertial forces if on a curved

CONTACT J.Z. Jiang. Email: z.jiang@bristol.ac.uk

track, which causes discomfort to the driver and influences manoeuvrability. Passive absorbers, viscous dampers in parallel with suspension springs, have been widely used to suppress these vibrations. To achieve better ride quality and road handling, semi-active and active suspensions have been explored by many researchers. Semi-active elements, such as the MR damper and the ER damper were proposed to be used in vehicle suspensions, of which the damping coefficient can be adjusted within a large actuation bandwidth [1,2]. Moreover, theoretical analysis and experimental validations have been carried out to investigate the advantages of the actively controlled passenger vehicles, such as in [3–5]. Despite the potential benefits of active or semi-active suspension struts, potential issues remain regarding the control-induced instability and larger control effort requirements.

In the field of passive vibration suppression, the inerter is a relatively new element [6]. It has the property that the applied force is proportional to the relative acceleration between its two terminals. The introduction of the inerter completes the analogy between mechanical and electrical systems, allowing all the positive-real immittance functions to be realised by the passive networks consisting of inerters, dampers and springs. Performance benefits from employing inerters have been identified for various mechanical systems, including vehicle suspensions [7–12], motorcycle steering systems [13], train suspension [14,15], buildings [16,17] and landing gears [18]. The application of the inerter in passive suspension systems was first investigated in [7], where six networks were proposed as suspension candidate layouts. It has been shown that improvements in ride comfort, tyre grip and dynamic load carrying capability of about 10% or greater can be obtained for a quarter-car model. Papageorgiou and Smith [8] proposed an approach, in which a fixed-order positive-real immittance functions with Linear Matrix Inequalities was optimised. This approach led to a further performance improvement for the same quarter car model. In [10], by considering suspension travel as a performance measure, it was illustrated that the suspension deflection is the more fundamental limitation for both ride comfort and tyre grip performance for passenger vehicles. An experimental study has been reported in [9], demonstrating the effectiveness of an inerter-based suspension device, on improving performance of passenger vehicles.

Despite the significant performance benefits that have been identified for passenger vehicles in previous studies, these potential benefits are yet to be realised in industry. This is because firstly, in previous investigations, some important practical performance constraints have not been taken into consideration, such as high-frequency dynamic stiffness which influences the NVH performance and frequency content consideration of the sprung mass acceleration which more directly relates to passenger perception. Secondly, most of the previous works, for example, [7,9–11] were limited to simple passive configurations, which inevitably restrict the achievable performance of inerter-based suspension devices. The remaining works, i.e. [8] can cover a larger range of network possibilities by using the immittance functions, however they may result in complicated configurations with exceeded element numbers and parameter values. As an example, some positive-real bicubic immittance require the Bott-Duffin synthesis [19], which corresponds to the series-parallel networks with thirteen elements. In this paper, the structure-immittance approach, proposed in [20], is adopted for identifying the beneficial suspension configurations. This approach can not only cover all network possibilities with pre-determined numbers of each element type, but can also include explicit information of network topology and element values. By selecting the passenger ride comfort with frequency content consideration as the key performance index, the other important performance measures including the suspension travel, the

tyre load and the high-frequency dynamic stiffness are imposed as hard constraints that the resulting suspension configurations must provide equivalent or better level of performance as the conventional one. In addition, a damper top mount, commonly used in vehicles to provide ideal Noise-Vibration-Harshness (NVH) performance [21], is also included in the considered quarter-car model.

This paper is structured as follows. In Section 2, a quarter-car model with damper top mount is introduced, together with the candidate suspension layouts formulated using the structure-immittance approach. The performance measures and the optimisation constraints are also provided and presented. In Section 3, the baseline performance is firstly obtained by considering a quarter-car model with a conventional suspension strut. For the ride comfort index, several inerter-based suspension configurations are then identified, with which the tyre load and suspension travel performance measures are then checked. In Section 4, constraints on both tyre load and suspension travel are implemented in the optimisation process, to make sure our analysis is in practical scenarios. Sensitivity analysis regarding the quarter-car parameter changes is then investigated for selecting the beneficial suspension struts. Time domain verification and reality check are finally carried out, to show the feasibility of the proposed suspension configurations. Conclusions are drawn in Section 5.

2. Quarter-car model, suspension strut and performance measure

2.1. Quarter-car model with damper top mount

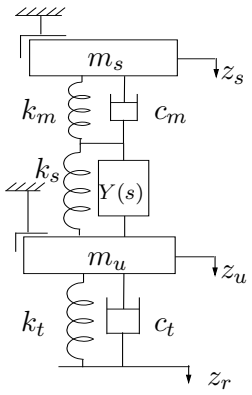

Figure 1. A quarter model with a damper top mount.

A standard model for developing suspension systems is the quarter-car model shown in Figure 1 with a sprung mass m_s, an unsprung mass m_u and a tyre modelled as a linear stiffness k_t and viscous damping c_t. The suspension strut consists of a suspension spring k_s and a passive absorber represented by a mechanical admittance $Y(s)$, where $Y(s) = F(s)/V(s)$ is the transfer function from the relative velocity $V(s)$ across the terminals to the force $F(s)$ exerted to the terminals in the Laplace domain. The suspension strut is attached on the unsprung mass and connected with the sprung mass through a damper top mount, which is commonly used in passenger vehicles to enhance the noise-vibration-harshness (NVH) performance. Here we consider the top mount as a linear spring k_m and a damper c_m based on previous work, such as [22]. The quarter-car parameters used in this study are listed in Table 1.

Table 1. Quarter car model parameters.

Parameter	Value	Unit
Sprung mass m_s	250	kg
Unsprung mass m_u	40	kg
Suspension stiffness k_s	30	kN/m
Tyre stiffness k_t	200	kN/m
Tyre damping c_t	270	Ns/m
Top mount stiffness k_m	200	kN/m
Top mount damping c_m	270	Ns/m

2.2. A traditional damper and Candidate layouts

Following [23], a traditional linear damper c_s with 0.25 damping ratio is selected as the default suspension strut, as shown in Figure 2(a), where c_s equals 1.37 kNs/m. The

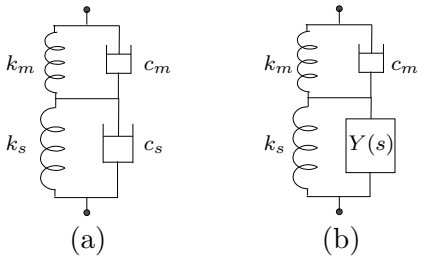

Figure 2. A suspension strut with top mount of (a) the traditional susepsnion strut and (b) the candidate layouts.

candidate layouts considered here are the networks consisting of inerters, dampers and springs with pre-determined numbers of each element type. Given any element number included in the candidate layout, all the series-parallel network possibilities can be covered by the generic networks, formulated with the structure-immittance approach [20]. The force-velocity immittance functions of the generic networks are then derived as $Y(s)$ of Figure 2(b) for optimisation. In this paper, we consider networks with up to six elements, divided into eight cases, which are (i) three-element networks, i.e. 1b1c1k case, (ii) four-element networks with 1b1c2k, 1b1k2c and 1c1k2b cases, (iii) five-element networks including 1b2c2k, 1c2b2k and 1k2b2c cases, and (iv) six-element networks considering 2b2c2k case, where 1, 2 represent the element numbers and b, c, k correspond to the inerter(s), damper(s) and spring(s).

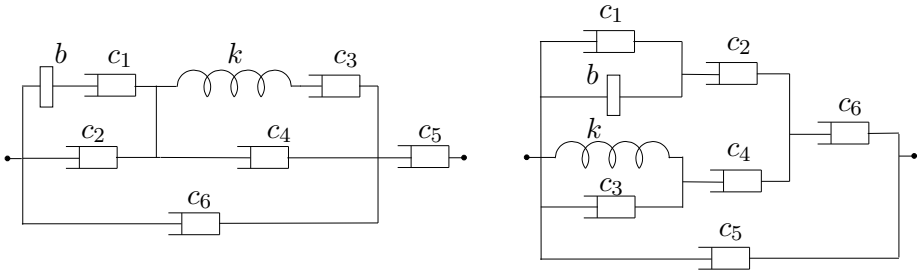

Figure 3. Generic networks for the case with one inerter, one spring and two dampers.

Taken the 1b1k2c case as an example, based on the formulation procedure shown in Figure 5 of [20], two generic networks can be obtained as Figure 3. These two networks, along with the constraints that at most two dampers exist, cover all 18

network layout possibilities. Their corresponding force-velocity immittance functions can be calculated as

$$Y_i(s) = \frac{n_i(s)}{m_i(s)} \quad (i = 1,\ 2) \tag{1}$$

with

$$n_1(s) = b(c_4 + c_6)s^2 + (bk(\frac{c_2}{c_1} + \frac{c_6}{c_1} + \frac{c_4}{c_3} + \frac{c_6}{c_3} + 1) + c_2c_4 + c_2c_6 + c_4c_6)s + k(c_2 + c_6),$$

$$m_1(s) = b(\frac{c_2}{c_1}+\frac{c_4}{c_1}+\frac{c_4}{c_5}+\frac{c_6}{c_5}+1)s^2+(bk(\frac{1}{c_1}+\frac{1}{c_3}+\frac{1}{c_5})+c_2+c_4)s+k(\frac{c_2}{c_3}+\frac{c_2}{c_5}+\frac{c_4}{c_3}+\frac{c_6}{c_5}+1)$$

$$n_2(s) = b(\frac{c_3}{c_2}+\frac{c_5}{c_2}+\frac{c_3}{c_4}+\frac{c_5}{c_6}+1)s^2+(bk(\frac{1}{c_2}+\frac{1}{c_4})+c_1+c_3+c_5)s+k(\frac{c_1}{c_2}+\frac{c_1}{c_4}+\frac{c_5}{c_4}+\frac{c_5}{c_6}+1)$$

$$m_2(s) = b(\frac{1}{c_2} + \frac{1}{c_6})s^2 + (bk(\frac{1}{c_2c_4} + \frac{1}{c_2c_6} + \frac{1}{c_4}c_6) + \frac{c_1}{c_2} + \frac{c_1}{c_6} + \frac{c_3}{c_4} + \frac{c_3}{c_6} + 1)s + k(\frac{1}{c_4} + \frac{1}{c_6})$$

where $b \geq 0,\ k \geq 0$ and for $i = 1$, corresponding to the left-hand generic network in Figure 3, at least four of parameters $1/c_1,\ c_2,\ 1/c_3,\ c_4,\ 1/c_5,\ c_6$ equal zero, whereas with $i = 2$, corresponding to the right-hand network in Figure 3, at least four of parameters $c_1,\ 1/c_2,\ c_3,\ 1/c_4,\ c_5,\ 1/c_6$ equal zero. These two immittance functions with the imposed parameter conditions can then be used for further optimisation.

2.3. Performance measures and constraints

There are a number of practical design requirements for a suspension system such as passenger comfort, tyre load, suspension travel and NVH performance. Ride comfort, an important performance measure depending on the acceleration level, frequency, direction and position, is selected as the key performance index in this paper. The ISO 2631 standard specifies a method to evaluate the effect of exposure to vibration on humans by weighting the acceleration with human vibration-sensitivity curves. The frequency weighting curve for vertical acceleration (measured at the seat surface) has been provided in the ISO 2631 standard, and a second-order shape filter of the form

$$H_{2631}(s) = \frac{50s + 500}{s^2 + 50s + 1200} \tag{2}$$

has been used in [23] to approximate the ISO weighting curve, which is also adopted here for measuring the ride comfort index. In addition, it is pointed out in [24] that vehicle ride comfort can be evaluated by using the vertical acceleration of the body up to 20Hz, while the higher frequency response is more related to the NVH performance. Based on [25], the secondary ride, vibrations in the frequency range from 4Hz to 20Hz, relates most to the ride comfort, and the primary ride (frequency range from 0Hz to 4Hz) is generally associated with rigid body movements. Using these observations, for

improving the passenger ride comfort performance, we propose an objective function J_r, expressed by

$$\begin{aligned} J_r &= \int_{w_1}^{w_2} |T_{\dot{z}_r \to \ddot{z}_s}(j\omega) H_{2631}(j\omega)|^2 S_{\dot{y}} d\omega \\ &\approx \Delta\omega S_{\dot{y}} \sum_{w_1}^{w_2} |T_{\dot{z}_r \to \ddot{z}_s}(j\omega) H_{2631}(j\omega)|^2 \end{aligned} \tag{3}$$

where $w_1 = 8\pi$, $w_2 = 40\pi$ represents the secondary ride frequency range of [4Hz, 20Hz], $T_{\dot{z}_r \to \ddot{z}_s}$ denotes the transfer function from the road velocity input $\dot{z}_r$ to the sprung mass acceleration $\ddot{z}_s$ and

$$S_{\dot{y}} = 2\pi\kappa V$$

is the power spectra of the road velocity input with κ, V representing the road roughness factor and vehicle speed, respectively. In this study, we select $V = 25$ m/s and $\kappa = 5\times10^{-7}$ m^{3}cycle^{-1}, in line with [7,8]. Also note that in the following discussion, we denote $|T_{\dot{z}_r \to \ddot{z}_s}(j\omega) H_{2631}(j\omega)|$ as weighted sprung mass acceleration a_{m_s} for simplicity. For the tyre load performance measure, the rms tyre load parameter J_t is defined as

$$J_t = 2\pi(V\kappa)^{1/2} ||T_{\dot{z}_r \to k_t(z_u - z_r)}||_2 \tag{4}$$

and the suspension travel performance measure can be represented by the maximum relative movement of the suspension strut, expressed by

$$J_s = (2\pi V\kappa)^{1/2} ||T_{\dot{z}_r \to (z_s - z_u)}||_\infty \tag{5}$$

Considering the vehicle NVH performance relating to the high-frequency dynamic stiffness, it has been proposed in [26] that a higher dynamic stiffness of the suspension strut will provide a poorer NVH performance. Hence, we impose a constraint that the dynamic stiffness of the suspension candidate layouts, denoted as K_{dyn}, should be no larger than the default one in the frequency range above 20Hz. For the primary ride vibrations in the frequency range of [0Hz, 4Hz], to ensure similar level of rigid body movement of the quarter-car model, another constraint is proposed, that within the primary ride frequency range, the maximum magnitude of the weighted sprung mass acceleration, denoted as $\max(a_{m_s})$ and its corresponding frequency $f|_{a_{m_s}=\max(a_{m_s})}$ should be within the range [95%, 105%] of the default values for the traditional suspension strut.

3. Optimisation results without tyre load and suspension travel constraints

In this section, the networks consisting of up to four elements are taken as candidate layouts, i.e. 1b1c1k, 1b1c2k, 1b1k2c and 1c1k2b cases. The response of the quarter-car model with the traditional damper is treated as the baseline. Optimisations are carried out for improving the ride comfort performance, satisfying the constraints on primary ride and suspension dynamic stiffness. The identified suspension configurations are then assessed using tyre load and suspension travel performance measures, suggesting

the necessity of imposing constraints on both of these in designing the suspension devices.

3.1. Baseline performance and optimisation procedure

For the default suspension strut, shown in Figure 2(a), the frequency response of the weighted sprung mass acceleration is presented in Figure 4(a), where two short vertical dashed lines show the frequency boundaries of primary and secondary ride. It can be

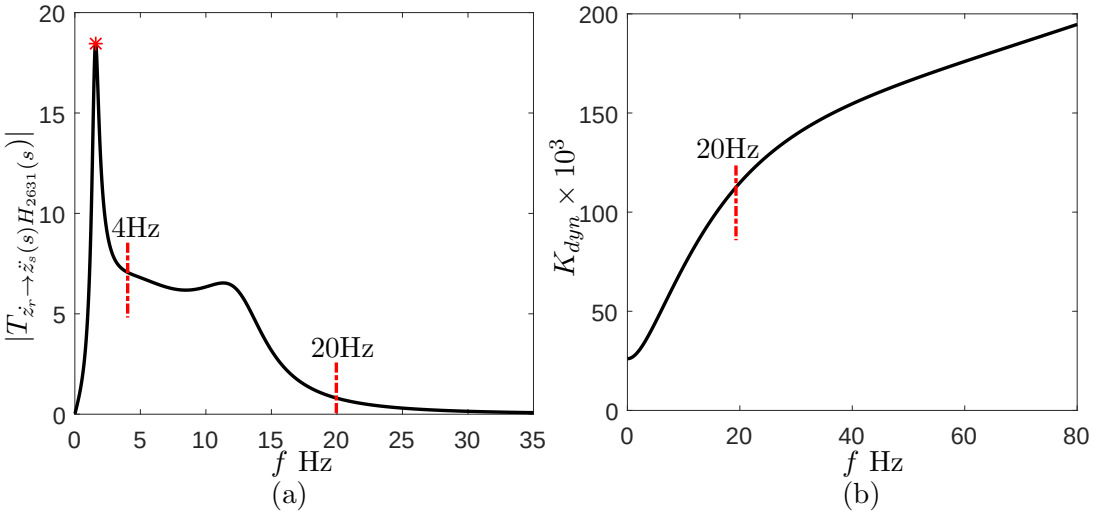

Figure 4. Frequency response with the default suspension device of (a) weighted sprung mass acceleration, (b) dynamic stiffness.

calculated that with this traditional suspension strut, the value of the ride comfort objective function J_r (3) is 0.211. It can also be noted from Figure 4(a) that the default primary ride maximum weighted acceleration and corresponding frequency is $\max(a_{m_s}) = 18.46$ and $f|_{a_{m_s}=\max(a_{m_s})} = 1.58$ Hz, shown as red star in Figure 4(a). Hence the constraint considering the primary ride vibrations, discussed in the previous section can be mathematically expressed as:

$$\frac{|\max(a_{m_s}) - 18.46|}{18.46} \leq 5\%, \quad \frac{|f|_{a_{m_s}=\max(a_{m_s})} - 1.58|}{1.58} \leq 5\% \tag{6}$$

Figure 4(b) shows the dynamic stiffness of the traditional suspension strut of Figure 2(a), which is the magnitude of its force-displacement transfer function, represented as $|\frac{(k_m+c_m s)(k_s+c_s s)}{k_m+k_s+s(c_m+c_s)}|$. The frequency range of vibrations related to the vehicle NVH performance is also predicted by the short vertical dashed line in Figure 4(b). From it, we can express the dynamic stiffness constraint as (7) with $Y(s)$ representing the force-velocity transfer function of the suspension candidate layouts.

$$|\frac{(k_m + c_m s)(k_s + Y(s)s)}{k_m + k_s + s(c_m + Y(s))}| \leq |\frac{(k_m + c_m s)(k_s + c_s s)}{k_m + k_s + s(c_m + c_s)}| \quad \text{when } s \geq 20 \text{ Hz} \tag{7}$$

Note that the static stiffness of the traditional suspension strut (Figure 2(a)) is $K_{\text{static}} = 26.09$ kN/m, which equals $(k_m^{-1} + k_s^{-1})^{-1}$. This static stiffness is used to ensure the suspension strut is capable of supporting the car body. In this work, the

optimisation will be conducted for the case that the static stiffness of each candidate layouts should be no smaller than this default value, while the suspension stiffness k_s can be optimised. For all the optimisations carried out in the present work, we use the MATLAB command *patternsearch* first and then *fminsearch* for fine-tuning of the parameters. It should be noted that the *patternsearch* and *fminsearch* functions require a set of initial values of the design variables, and their efficiency is dependent on the setting of the initial values. However, if the initial values are given properly, *patternsearch* and *fminsearch* functions are more accurate and faster than those global optimum design methodologies, which do not need to set any initial values, such as the genetic algorithm. To derive a global optimisation result by the *patternsearch* and *fminsearch* functions, a number of sets of initial values can be given in terms of random numbers in a considered value range, and then, the obtained values of the variables that would provide the objective function J_r with minimum value would be the global optimum parameters. Note that, during the optimization process, no restriction due to practical implementation consideration is placed on the parameter values. Instead, we consider whether the parameter values are practical after the optimization stage.

3.2. Identified suspension configurations

Considering all the possible networks with up to four elements, the optimal configurations are shown in Figure 5, together with the optimisation results summarised in Table 2. Note that the traditional suspension strut of Figure 2(a), denoted as Default in Table 2, is also optimised for the sake of comparison. The optimised traditional suspension strut is denoted as S1, with the value of the objective function J_r obtained as 0.1994. It can be seen that S1 can only provide limited performance advantage, approximately 5.2% better than the default one.

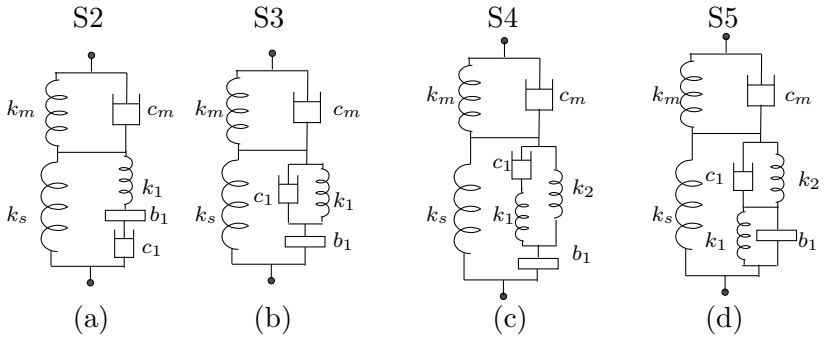

Figure 5. Suspension configurations idenftied for improving the ride comfort performance.

Table 2. Optimum results with the identified suspension configurations.

Configuration	Performance J_r (imp %)	Parameter values (kg, kNs/m, kN/m)
Default	0.2105 (-)	$c = 1.37,\ k_s = 30$
S1	0.1994 (5.2%)	$c = 1.29,\ k_s = 30$
S2	0.1442 (31.5%)	$b = 87.2,\ c = 1.19, k_1 = 9.6\ k_s = 30$
S3	0.1013 (46.3%)	$b = 95.7,\ c = 0.49, k_1 = 6.2\ k_s = 30$
S4	0.1011 (51.9%)	$b = 60.3,\ c = 0.29,\ k_1 = 792.02,\ k_2 = 4.99,\ k_s = 30$
S5	0.1005 (52.2%)	$b = 101.8,\ c = 0.39,\ k_1 = 2.29,\ k_2 = 5.35,\ k_s = 30$

For the case where the suspension device includes one inerter, one damper and one spring, out of the eight possible layouts (enumerated in [20]), the optimisation

indicates that two networks S2 and S3 shown in Figure 5(a) and (b) are optimal. With these two configurations, up to 46.3% performance improvement in ride comfort can be obtained. By allowing two springs in the suspension struts, the networks S4 and S5 are obtained as optimal configurations, providing 51.9% and 52.2% smaller value of ride comfort cost function J_r, respectively. The other two cases, i.e. 1b1k2c and 1c1k2b do not result in any better performance comparing with the 1b1c1k case. This means the additional damper in the 1b1k2c case or an inerter in 1c1k2b case always effectively disappears during the optimisation with its value turning to zero if it is connected in parallel or to infinity if connected in series. The frequency response of the weighted sprung mass acceleration with the identified configurations are shown in Figure 6(a), from which it can be seen that all the identified suspension configurations satisfy the constraints that the maximum sprung mass acceleration and its corresponding frequency should be similar to the default ones. Figure 6(b) shows the dynamic stiffness of the obtained configurations, suggesting that their dynamic stiffness is smaller than that of the default structure when the frequency is larger than 20Hz. Note that the configuration S5 has been proposed by Smith & Wang [7] for improving the ride comfort. However, the other three beneficial configurations of Figure 5(a-c), which can also provide significant performance benefits in ride comfort, have not been considered, previously.

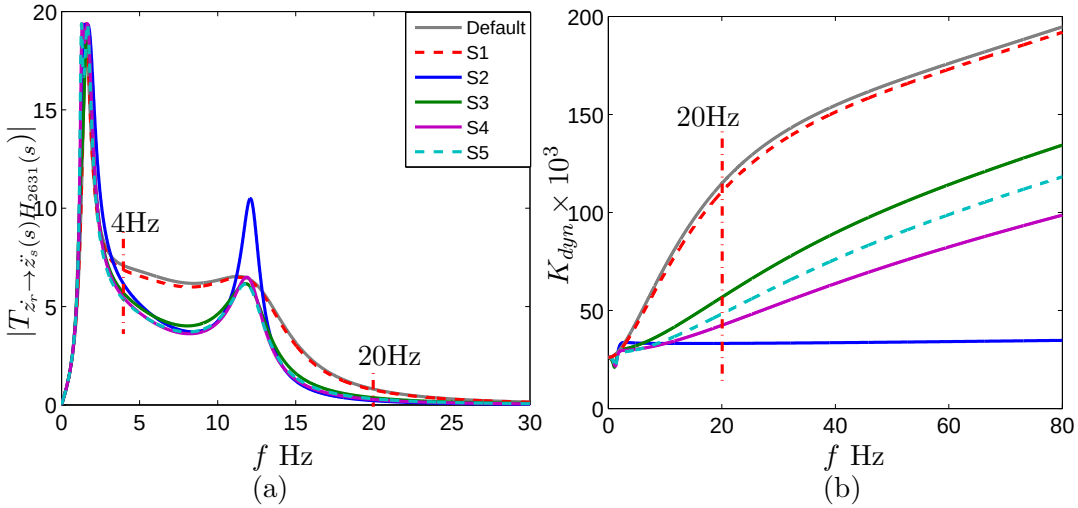

Figure 6. Frequency response of (a) weighted sprung mass acceleration, (b) dynamic stiffness with configurations S1-S5 and the default suspension device.

3.3. Analysis on tyre load and suspension travel with identified configurations

Up to this point, we have considered the ride comfort using the objective function J_r, the tyre load and suspension travel performance measures are now checked for the identified configurations. For the default suspension strut, based on (4) and (5), the tyre load and suspension travel can be calculated as $J_t = 559$ and $J_s = 0.0025$, respectively.

Table 3 provides the values of J_t and J_s for the optimal configurations S1 to S5, showing that the tyre load and suspension travel of the obtained configurations are significantly larger than the default structure. Note that with configuration S2, the tyre load is almost twice the default value, and configuration S5 results in around a 50%

Table 3. Tyre load and suspension travel values of the identified suspension configurations.

Configuration	Tyre load J_t	Suspension travel J_s
Default	559	0.0025
S1	579.4	0.0026
S2	1040	0.0031
S3	720	0.0026
S4	820	0.0036
S5	780	0.0039

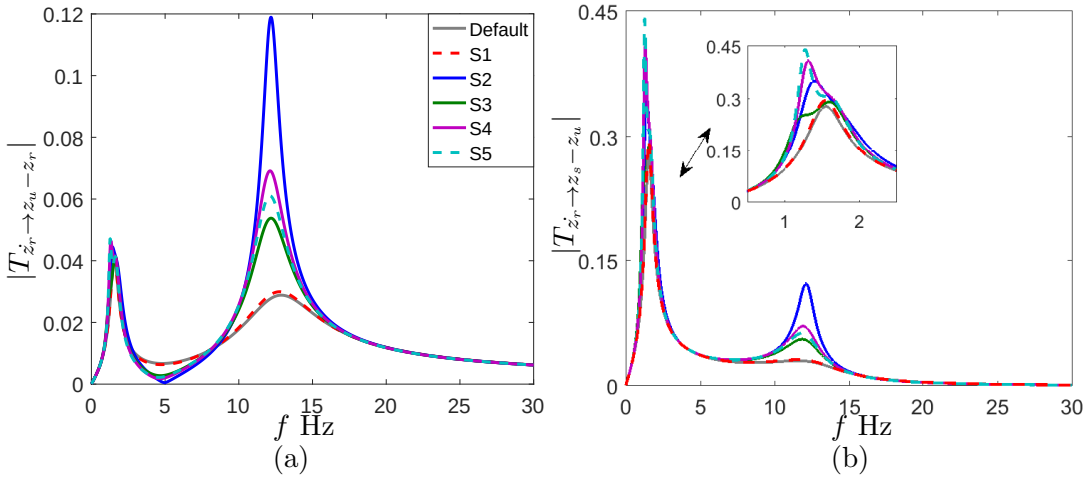

Figure 7. Frequency response of (a) tyre displacement $z_u - z_r$, (b) suspension movement $z_s - z_u$.

larger value of suspension travel J_s. The frequency response of the tyre displacement $z_u - z_r$ and the suspension movement $z_s - z_u$ is shown in Figure 7. It can be seen from Figure 7(a) that the suspension configurations S1-S5 result in larger tyre displacement around the second fundamental frequency of the quarter car model, 12 Hz. Also note from Figure 7(b), the maximum suspension displacement of the default suspension is significantly smaller than those of the identified configurations, as expected from Table 3. These inferior behaviours in tyre load and suspension travel with the obtained optimal suspension configurations will pose challenge for practical applications. Hence, constraints on tyre load and suspension travel will be implemented in the next section.

4. Beneficial suspension configuration identification

Further investigations with two extra constraints on tyre load and suspension travel are discussed in this section. It will be shown that, with these constraints, limited performance improvement in ride comfort is obtained when considering the suspension devices proposed in previous works [7,8]. By allowing up to six element numbers included in suspension strut, significant performance advantages can be identified using the structure-immittance approach. With the obtained suspension configurations, a sensitivity analysis is conducted considering changes in vehicle parameter values, to identify which beneficial configurations are robust. Note that while a 6 element device would be complicated to implement purely mechanically, it has been shown that the use of fluid-based inerter can provide integrated device solutions [27] with much reduced complexity.

4.1. Optimisation results with tyre load and suspension travel constraints

The tyre load J_t and the suspension travel J_s of the candidate layouts are constrained to be no larger than the default strut, i.e. $J_t \leq 559$ and $J_s \leq 0.0025$, which are implemented in the optimisation procedure. By minimising the ride comfort objective function J_r with the two additional imposed constraints, the optimal results and the corresponding strut configurations are summarised in Table 4 and Figure 8, for the candidate network layouts including up to six elements (the subscript k is used to indicate optimisation with both tyre load and suspension travel constraints). For comparison, the optimal configurations proposed in previous works, i.e. S6 of [7] and a positive-real biquadratic function in [8] are also considered, of which the optimisation results are shown in Table 5.

Table 4. Optimisation results considering the tyre load and suspension travel constraints.

Configurations	Performance J_r (imp %)	Parameter values (kg, kNs/m, kN/m)	Tyre load J_t	Suspension travel J_s
Default	0.211 (-)	$c = 1.37,\ k_s = 30$	559	0.0025
$S1_k$	0.211 (0%)	$c = 1.37,\ k_s = 30$	559	0.0025
$S2_k$	0.205 (2.7%)	$b = 87.2,\ c_1 = 1.19,$ $k_1 = 9.6\ k_s = 30$	559	0.0025
$S3_k$	0.190 (9.7%)	$b_1 = 167.6,\ b_2 = 141.7$ $c_1 = 1.34,\ k_1 = 12.89,$ $k_s = 30$	559	0.0025
$S4_k$	0.189 (10.1%)	$b_1 = 123.8,\ b_2 = 140.1,$ $c_1 = 1.34,\ k_1 = 2.67,$ $k_2 = 13.9,\ k_s = 30$	559	0.0024
$S5_k$	0.187 (11.4%)	$b_1 = 29.5,\ b_2 = 175.4,$ $c_1 = 1.27,\ c_2 = 1.08,$ $k_1 = 71.8,\ k_2 = 10.4,$ $k_s = 30$	559	0.0022
$S6_k$	0.185 (12.1%)	$b_1 = 40.6,\ b_2 = 6.08,$ $c_1 = 0.79,\ c_2 = 0.23,$ $k_1 = 57.8,\ k_2 = 3.68,$ $k_s = 30$	559	0.0023
$S7_k$	0.183 (13.3%)	$b_1 = 7.40,\ b_2 = 228.03,$ $c_1 = 1.01,\ c_2 = 0.98,$ $k_1 = 8.18,\ k_2 = 54.91,$ $k_s = 32.4$	559	0.0025

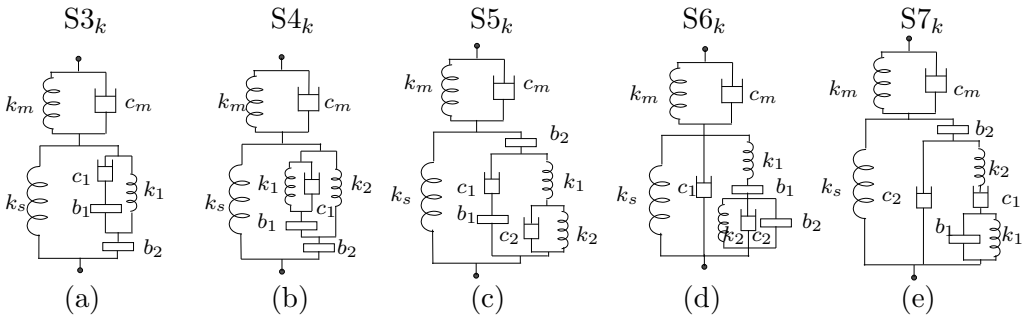

Figure 8. The identified optimal configurations $S3_k$ - $S7_k$.

It can be seen from Table 4 that when satisfying the constraints on tyre load and suspension travel, the performance improvement in terms of ride comfort index has been significantly reduced and different layouts are now optimised, compare the 4 element device $S3_k$ to those in Figure 5, S4 and S5. It can be noted that the suspension strut with a traditional damper, denoted as $S1_k$ is unable to provide a better perfor-

Table 5. Optimisation results with the previously proposed suspension layouts [7,8]

Configurations	Performance	element numbers required
S6 in [7]	0.205 (2.7%)	4
Biquadratic immittance in [8]	0.204 (3.1%)	9

mance than the default one. The configuration $S2_k$ has the same topology as absorber S3, shown in Figure 5(c). It can still provide a better ride comfort than the default even when required to satisfy the tyre load and suspension travel constraints, but the performance improvement is reduced from 46.3% to 2.7%. For the case where the suspension device includes four elements, i.e. the 1b1c2k, 1b1k2c and 1c1k2b cases, out of the 54 possible layouts obtained using the structure-immittance approach, network $S3_k$, consisting of two inerters, one damper and one spring is obtained as the optimum configuration, shown in Figure 8(a). With this strut, the value of J_r is obtained as 0.190, around 9.7% smaller than that of the default one. Note that the previously obtained beneficial configuration S4 and S5 in Section 3.1 both reduce to the S3 ($S2_k$) layout during the optimisation with the additional constraints applied, with k_1 of S4 turning to infinity and that of S_5 to 0. This means that with the additional spring, the ride comfort can be improved but its presence has a deleterious effect on the performance in tyre load and suspension travel. Consider the network possibilities consisting of five elements, configuration $S4_k$ is optimised, with a slightly improved performance over that of $S3_k$. By allowing two inerters, two dampers and two springs in the suspension device, the optimisation results indicate that three networks $S5_k$, $S6_k$ and $S7_k$ are all near optimal. Figure 8(c), (d) and (e) show these layouts. The strut $S7_k$ provides the best ride comfort performance, resulting in 13.3% smaller value of the objective function J_r comparing with the default structure. Considering the suspension devices proposed in previous works [7,8], it can be seen from Table 5 that the S6 in [7] provides very limited performance benefit, approximately 2.7% better than the default one. However, for the network with similar level of complicity (the included element number is the same, i.e. 4), the $S3_k$ identified in this paper can provide 9.7% performance advantage, almost five times that of S6 in [7]. Using the positive-real biquadratic immittance as a candidate layout [8], the performance improvement is also very limited, around 3.1%, while its realisation requires 9 elements. For the positive-real bicubic function, its potential performance improvement can be larger, however, 13 elements are required for its realisation, which is arguably too complicated for practical implementation.

The frequency response of the weighted sprung mass acceleration using these configurations is presented in Figure 9(a), and the dynamic stiffness is shown in Figure 9(b). It can be seen that configuration $S7_k$ results in the smallest maximum value of sprung mass acceleration across the frequency range approximately from 5Hz to 14Hz, while for the frequency range of [13Hz, 20Hz] it results in larger sprung mass accelerations than those using the default device. Also from Figure 9(b), we notice that the dynamic stiffness of $S6_k$ and $S7_k$ is larger than the default strut when the frequency is in the range of [11Hz, 20Hz], and for the frequency exceeds 20 Hz, its dynamic stiffness is significantly smaller than the default one. This predicts the superior NVH performance of the quarter car model with the suspension struts $S6_k$ and $S7_k$. The tyre load and suspension travel of the obtained configurations are also provided in Table 4, suggesting the constraints have been satisfied. Figure 10(a) and (b) shows the frequency response of the tyre displacement $z_u - z_r$ and the suspension movement

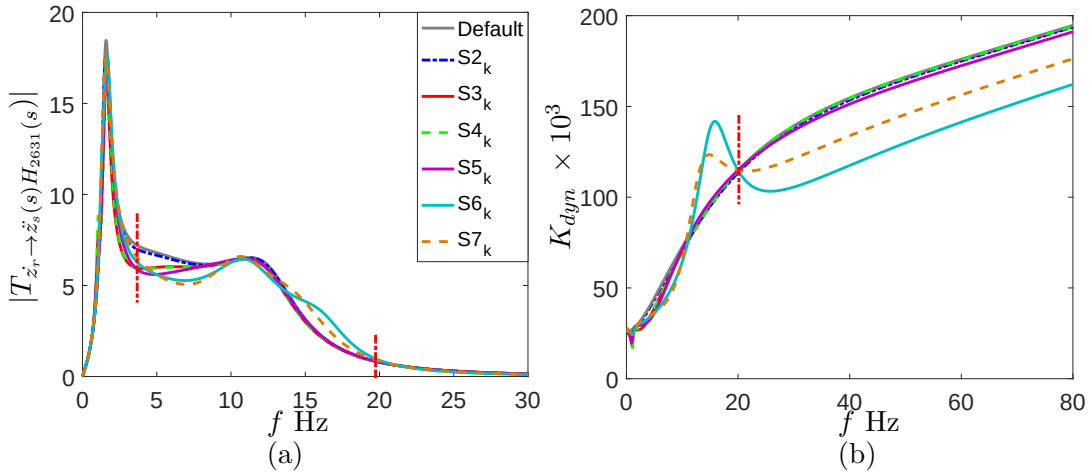

Figure 9. Frequency response of (a) weighted sprung mass acceleration, (b) dynamic stiffness with configurations $S2_k$- $S6_k$ and the default suspension strut.

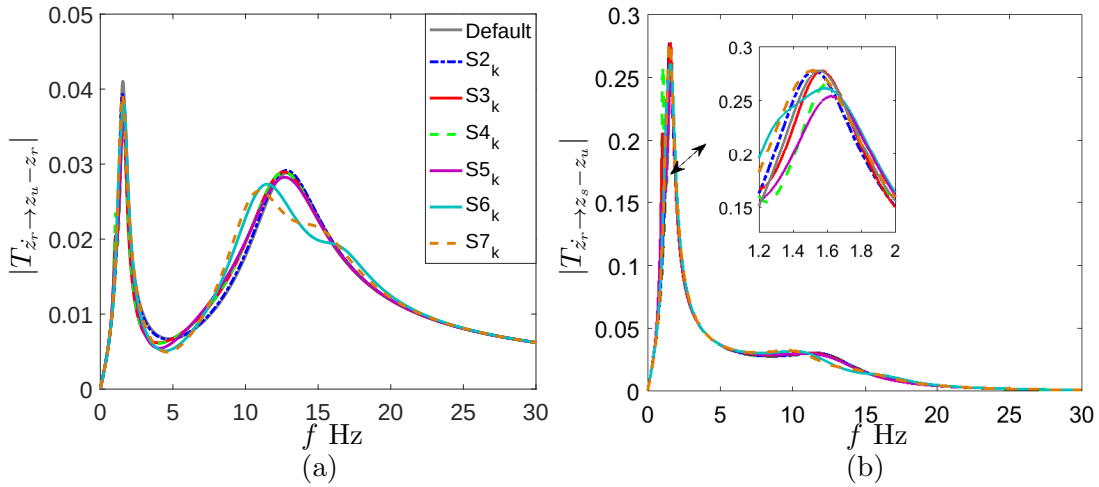

Figure 10. Frequency response of (a) tyre displacement $z_u - z_r$, (b) suspension movement $z_s - z_u$.

$z_s - z_u$ of the quarter car model with these obtained suspension configurations. It can be seen from Figure 10(a) that with all these configurations, the maximum tyre displacement is smaller than that of the default structure, and $S7_k$ provides the smallest tyre displacement around the second fundamental frequency. In addition, it can also be seen from Figure 10(b) that comparing with the default structure, all the obtained suspension configurations provide equivalent or smaller maximum value of suspension movement, as expected from Table 4.

4.2. Sensitivity analysis

Several suspension configurations have been identified for enhancing the passenger ride comfort while satisfying the constraints on high-frequency dynamic stiffness, tyre load and suspension travel performance measures. An important step in identifying a beneficial suspension configuration is to assess the robustness of the device to vehicle parameter changes via a sensitivity analysis. The quarter-car model of Figure 1 is varied to evaluate the suspension strut sensitivity to changes in the following pa-

rameters: sprung mass m_s and unsprung mass m_u, where the sprung mass m_s can be easily effected by the weight of passenger, cargo and the amount of gasoline, and the unsprung mass m_u is highly related with the tyre weight. The suspension robustness is evaluated using the three considered performance measures, i.e. the ride comfort J_r (3), the tyre load J_t (4) and the suspension travel J_s (5).

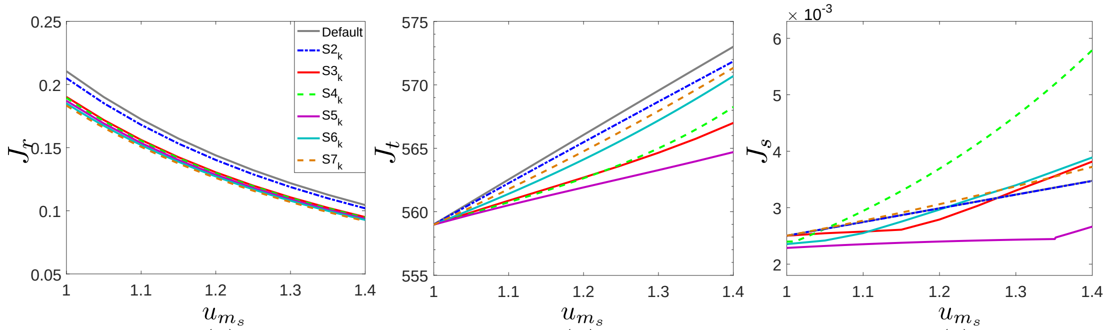

Figure 11. Performance values with respect to the sprung mass ratio u_{m_s} for (a) the ride comfort J_r, (b) the tyre load J_t and (c) the suspension travel J_s.

Considering the sprung mass m_s, the range of considered values are $u_{m_s} \times 250$ kg, where $u_{m_s} \in [1,\ 1.4]$ is the ratio between the changed sprung mass and the default value. The values of the considered performance measures are shown in Figure 11 with respect to the sprung mass ratio u_{m_s}, for all the proposed suspension configurations (without re-optimisation). It can be seen from Figure 11(a) that the changing trend of the ride comfort cost function J_r with the obtained suspension configurations S2$_k$ - S7$_k$ is similar to that with the default suspension strut - a larger sprung mass results in a lower value of J_r, which means a better ride comfort performance. Across the whole range of sprung mass values, the configuration S7$_k$ always provides the best ride comfort performance however the performance improvement is slightly reduced with larger values of sprung mass. Figure 11(b) shows that the value of tyre load J_t becomes larger with the increasing sprung mass and all the six proposed beneficial configurations provide better tyre load performance, comparing with the default strut, where the S5$_k$ outperforms all the other structures. It can also be seen that when the value of sprung mass increases, the beneficial configurations outperform the default one in terms of tyre load. The changing trend of the suspension travel versus the sprung mass is provided in Figure 11(c). The suspension travel J_s for S4$_k$ is significantly larger than the default one when the weight of sprung mass increases, hence we reject this configuration. In contrast, configuration S5$_k$ provides the smallest suspension travel value across all configurations over the full range of the sprung mass values considered. If a 5% degradation of the value of J_s is acceptable then in addition to S5$_k$, configurations S2$_k$, S3$_k$, S6$_k$ and S7$_k$ can all be considered as robust suspension struts to the change of the sprung mass, in the performance of suspension travel.

For the unsprung mass m_u, we take its value to be changed within the range $m_u \in [0.9,\ 1.1] \times 40$ kg, where we define the ratio between its changed value to the default one as u_{m_u}. The other parameter values of the quarter car model are kept unchanged. Figure 12 presents the values of the considered performance measures J_r, J_t and J_s with respect to the unsprung mass weights. From Figure 12(a), it can be seen that comparing with the default suspension strut, all the six identified configurations S2$_k$-S7$_k$ provides better ride comfort performance in the whole range of the unsprung mass values. Also configurations S6$_k$ and S7$_k$ result in larger performance improvement when

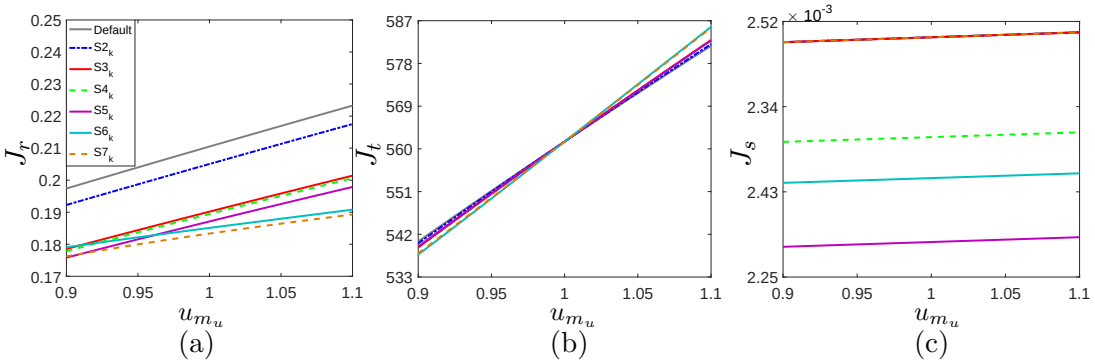

Figure 12. Performance values with respect to the unsprung mass ratio u_{mu} for (a) the ride comfort J_r, (b) the tyre load J_t and (c) the suspension travel J_s.

the unsprung mass becomes heavier. The values of tyre load J_t and suspension travel J_s are shown in Figure 12(b) and (c), respectively. Figure 12(b) suggests that the proposed beneficial suspension struts have similar tyre load performance to that of the default structure over the range of unsprung mass values considered. Also, from Figure 12(c), the suspension travel of the proposed configurations are only slightly effected by the change of the unsprung mass, and comparing with the default strut, the identified configurations still provide better suspension travel performance across the unsprung mass range.

In summary, five of the identified configurations, i.e. $S2_k$, $S3_k$, $S5_k$, $S6_k$ and $S7_k$ are the robust suspension strut designs, and because of the limited performance improvement achieved by $S2_k$, the other four configurations are considered as the beneficial suspension struts.

4.3. Time domain verification and reality check on beneficial suspension configurations

Finally, we consider the performance of the quarter-car model with the proposed beneficial suspension configurations subjected to a time-domain road input. In this subsection, we only consider configuration $S7_k$ as an example, (the other configurations can be analysed in a similar way). Following [28], we chose a road velocity input $\dot{z}_r$, defined in (8)

$$\dot{z}_r(t) = -0.111[Vz_r(t) + 40\sqrt{\kappa V}\tau(t)] \tag{8}$$

to capture a random road with roughness coefficient as $\kappa = 5 \times 10^{-7}\text{m}^3/\text{cycle}$, same as that used in previous optimisations. Here V is the vehicle velocity, taken as 25 m/s and $\tau(t)$ is the Gaussian white noise with mean value zero. With the suspension configuration $S7_k$, the time-domain response of sprung mass acceleration of the quarter-car model is shown as orange dashed line in Figure 13. The default response is also provided (black line) for comparison. It can be seen that the proposed configuration $S7_k$ results in smaller sprung mass accelerations most of time. The rms and maximum values of the sprung mass acceleration, tyre displacement and suspension movement with the $S7_k$ and the default suspension have been calculated in Table 6. From it, we can see that both rms and maximum sprung mass acceleration values for the $S7_k$ are approximately 9% smaller than the default values. This reflects the performance improvement of the $S7_k$ configuration over that of the default as obtained in previous

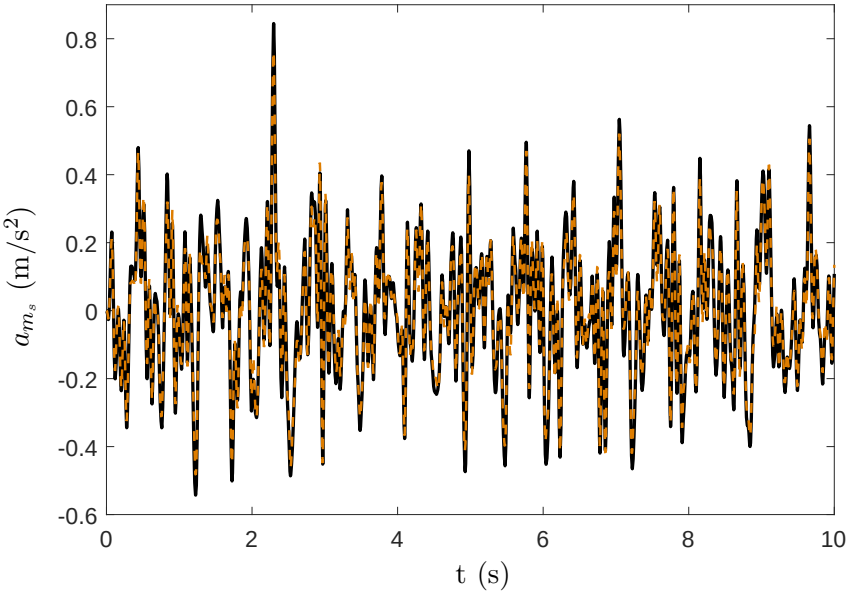

Figure 13. The time domain response of sprung mass acceleration under road input z_r (8) with the default suspension configuration (black solid) and S7$_k$ (orange dashed).

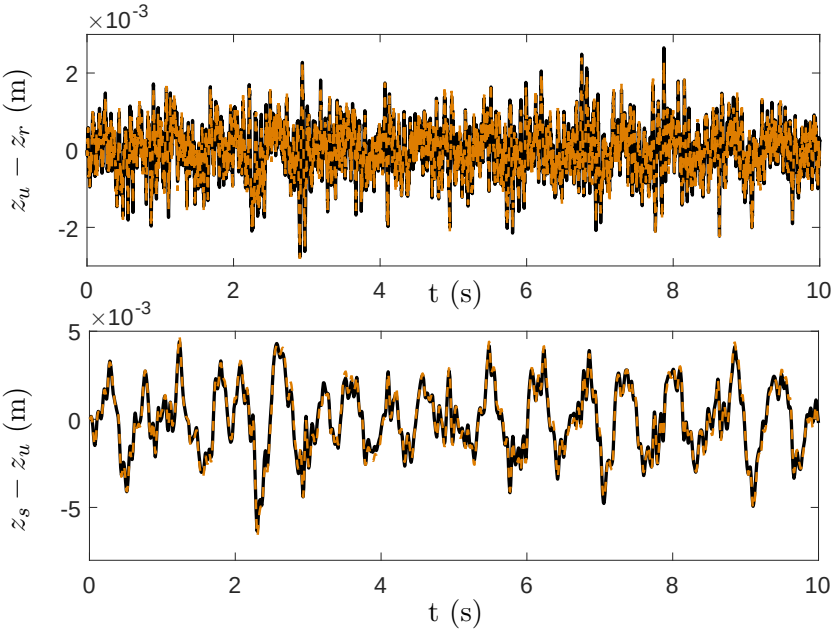

Figure 14. The time domain response of tyre displacement $z_u - z_r$ and suspension movement $z_s - z_u$ under road input z_r (8) with the default suspension configuration (black solid) and S7$_k$ (orange dashed).

analysis. Figure 14 presents the time domain response of tyre displacement $z_u - z_r$ and the suspension movement $z_s - z_u$. With this figure, it can be calculated that for the configuration S7$_k$, the rms value of tyre displacement is 0.645 mm and the maximum suspension travel is 6.6 mm, shown in Table 6. Considering the default structure, their values can be obtained as 0.647 mm and 6.4 mm, respectively. From these, we can obtain that the proposed beneficial configuration S7$_k$ have similar tyre load and

suspension travel performance with the default one, suggesting the effectiveness of implementing the constraints for frequency-domain optimisation.

Table 6. Average and maximum value of the sprung mass acceleration a_{m_s}, the tyre displacement $z_u - z_r$ and suspension movement $z_s - z_u$, subjected to a random road input (8).

Configurations	Average			Maximum		
	a_{m_s} m/s^2	$z_u - z_r$ mm	$z_s - z_u$ mm	a_{m_s} m/s^2	$z_u - z_r$ mm	$z_s - z_u$ mm
Default	0.200	0.647	1.9	0.845	2.8	6.4
S7$_k$	0.182	0.645	2.0	0.763	2.8	6.6

Finally, we check the power dissipation of the proposed beneficial suspension configurations, to make sure that no unexpected behaviour occurs. The power flow method proposed in [29] is adopted with a brief introduction provided here. The power flow is defined as $P = f(t) \cdot v(t)$ with $f(t)$ being the force loaded at a structure point and $v(t)$ as the velocity response of a point under the load $f(t)$. In frequency domain, a time average vibration power defined as

$$\bar{P} = \frac{1}{2}\mathrm{Re}(F \cdot V^*) \tag{9}$$

is used, where F, V represent the frequency response of the loaded force and the relative velocity, and the subscript $*$ denotes the complex conjugate. This equation is obtained based on an assumption that the dynamic system is forced by a harmonic excitation and the averaging time is a cycle of the periodic response. Using the equation (9), the input power $\bar{P}_{in}$ of the quarter car model is defined as

$$\bar{P}_{in} = \frac{V_r}{2}\mathrm{Re}((k_t + c_t s)(Z_u - \frac{V_r}{s})) \tag{10}$$

where $V_r = \sqrt{2\pi V \kappa}$ denotes the constant road velocity input $\dot{z_r}$ in frequency domain and Z_u is the displacement of the unsprung mass m_u. The power dissipated by the tyre damping, $\bar{P}_{ct}$ can be expressed as:

$$\bar{P}_{ct} = \frac{c_t}{2}\mathrm{Re}([(Z_u - \frac{V_r}{s})s] \cdot [(Z_u - \frac{V_r}{s})s]^*) \tag{11}$$

The power dissipated by the suspension devices can also be calculated based on (9), which also depends on their topological connection. For the configuration S7$_k$, its power flow is calculated and presented as orange dashed lines of Figure A1 in Appendix A, with (a), (b) and (c) representing the input power, the tyre and suspension dissipated power, respectively. For quantitatively representing the power flow distribution, the average and the maximum value of the power flow is calculated and summarised in Table A1, Appendix A. It can be seen that the average input power of the S7$_k$ and the conventional suspension strut is as the same as each other and for the maximum input power, the configuration S7$_k$ results in a smaller value. Also we notice that for the configuration S7$_k$, the tyre dissipated power $\bar{P}_{ct}$ is smaller, and the suspension dissipated power $\bar{P}_{sus}$ is larger than that of the default suspension. This can be regarded as beneficial since less tyre dissipated power means lower rolling resistance and higher fuel efficiency, as reported in [30].

Subsequently, a bump road input [3], one of the most extreme surface irregularities encountered is also considered. This is to ensure that while the beneficial suspension configurations are optimised for road profiles with specific road roughness coefficient, they will not result in inferior performance when subjected to more extreme road surfaces. Consider the bump road input shown in Figure A2, Appendix A, it takes the following mathematical expression:

$$z_r = \frac{H}{2} \times (1 - cos(\frac{2\pi v_h t}{L})) \tag{12}$$

where H, L are the bump height and width, taken as 0.07 m and 0.4 m, respectively. v_h is the vehicle operation speed with the value of 8.3 m/s. Subjecting the quarter car model to this road surface, the performance with the $S7_k$ in ride comfort is provided in Figure A3 (a), together with the default performance in black solid line. The tyre displacement and the suspension movement subjected to this bump road input are also presented in Figure A3 (b) and (c), respectively. Table A2 shown in Appendix A summarises the average and maximum values of these considered parameters. It can be noted both from Figure A3 and Table A2 that the quarter-car model with configuration $S7_k$ will not experience any unexpected behaviour when subjected to a bump input.

5. Conclusions

This paper has investigated the potential passenger comfort performance benefits in secondary ride using inerter-based suspension devices for a quarter car model with a damper top mount. Multiple performance requirements including primary ride performance and high-frequency dynamic stiffness have also been taken into consideration, formulated as optimisation constraints. Using the structure-immittance approach, up to 52% performance improvement has been identified with the optimal inerter-based configurations including at most four elements. An analysis on checking the tyre load and suspension travel was then carried out, showing significant undesirable behaviour occurs in these performance measures. Hence, extra constraints on tyre load and suspension travel were implemented for further optimisation, and the networks consisting of up to six elements were used as candidate suspension layouts. Six optimal configurations that provide up to 13.3% performance improvement were then obtained and presented making use of the structure-immittance approach. For these obtained configurations, sensitivity analysis against quarter-car model parameter changes have further been investigated. Four of the six optimal configurations were finally identified as beneficial suspension configurations. By selecting a random surface as road input, effectiveness of the proposed suspension configuration was verified in time domain analysis. Furthermore, energy dissipation of the proposed beneficial configurations and the quarter-car model response subjected to a bump road input were studied, suggesting the feasibility of the identified suspension configurations.

Appendix A. Figures and Tables for reality check

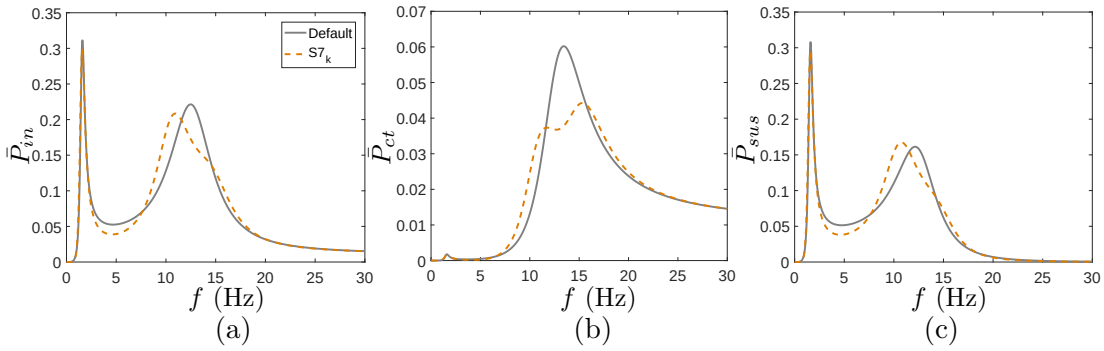

Figure A1. Time-average power flow of (a) input power $\bar{P}_{in}$, (b) tyre power dissipation $\bar{P}_{ct}$ and (c) suspension power dissipation $\bar{P}_{csus}$.

Table A1. Average and maximum value of the power flow.

Configurations	Average			Maximum		
	$\bar{P}_{in}$	$\bar{P}_{ct}$	$\bar{P}_{sus}$	$\bar{P}_{in}$	$\bar{P}_{ct}$	$\bar{P}_{sus}$
Default	0.072	0.0196	0.0524	0.3113	0.0602	0.3079
$S7_k$	0.072	0.0190	0.0530	0.2985	0.0442	0.2955

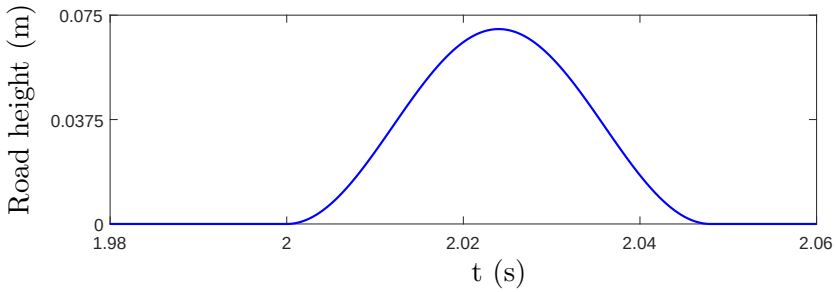

Figure A2. The bump road input.

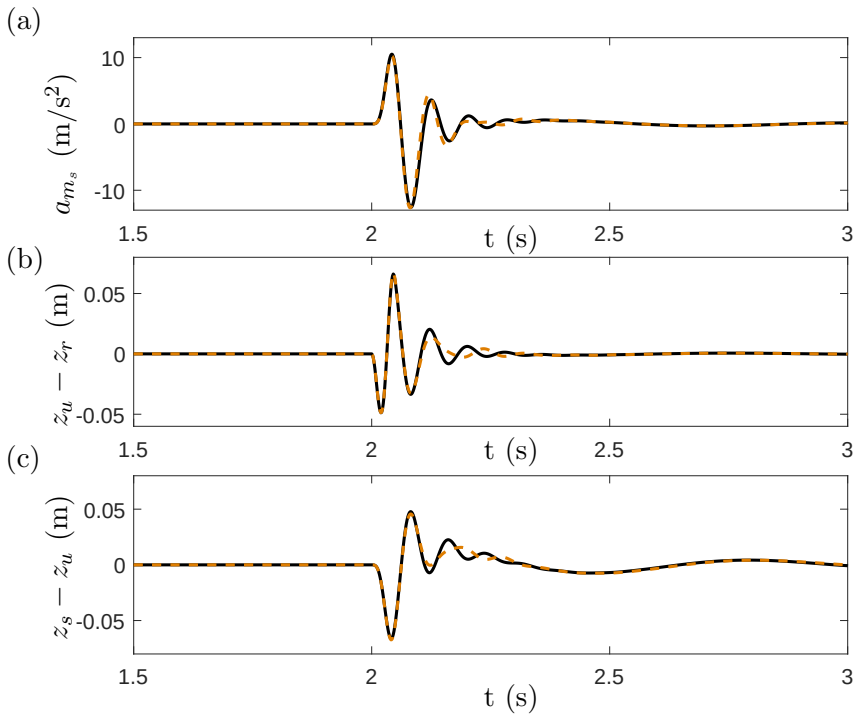

Figure A3. The time domain response of sprung mass acceleration, tyre displacement and suspension movement under bump road input with the default suspension strut (black solid) and S7$_k$ (orange dashed).

Table A2. Average and maximum value of the sprung mass acceleration a_{m_s}, the tyre displacement $z_u - z_r$ and suspension movement $z_s - z_u$, subjected to a bump input (12).

Configurations	Average			Maximum		
	a_{m_s} m/s^2	$z_u - z_r$ mm	$z_s - z_u$ mm	a_{m_s} m/s^2	$z_u - z_r$ mm	$z_s - z_u$ mm
Default	0.96	5.1	4.3	12.62	66.3	66.1
S7$_k$	0.93	5.0	4.2	12.66	66.9	66.8

Acknowledgement(s)

The authors would like to acknowledge the support of the EPSRC, the University of Bristol and Jaguar Land Rover: J.Z. Jiang and S.Y. Zhang are supported by an EPSRC First Grant EP/P013456/1. The authors are also grateful for the technical and financial support from Jaguar Land Rover.

References

[1] H. Du, N. Zhang, F. Naghdy, Robust control of vehicle electrorheological suspension subject to measurement noises, Vehicle System Dynamics, 2011.

[2] H. Du, K.Y. Sze, J. Lam, Semi-active H∞ control of vehicle suspension with magneto-rheological dampers, Journal of Sound and Vibration, 2005.

[3] H.P. Du, N. Zhang, H∞ control of active vehicle suspensions with actuator time delay, Journal of Sound and Vibration, 2007.

[4] H. Du, N.Zhang, J.Lam, Parameter-dependent input-delayed control of uncertain vehicle suspensions, Journal of Sound and Vibration, 2008.
[5] G. Priyandoko, M. Mailah, H. Jamaluddin, Vehicle active suspension system using skyhook adaptive neuro active force control, Mechanical Systems and Signal Processing, 2009.
[6] M.C. Smith, Synthesis of mechanical networks: the inerter, IEEE Transactions on Automatic Control, 2002.
[7] MC. Smith, FC. Wang. Performance benefits in passive vehicle suspensions employing inerters. Vehicle System Dynamics, 2004.
[8] C. Papageorgiou, MC. Smith. Positive real synthesis using matrix inequalities for mechanical networks: application to vehicle suspension. IEEE Transactions on Control Systems Technology, 2006.
[9] Y.J. Shen, L. Chen, X.F. Yang, D.H. Shi, J. Yang, Improved design of dynamic vibration absorber by using the inerter and its application in vehicle suspension, Journal of Sound and Vibration, 2016.
[10] Y.L. Hu, M.Z.Q. Chen, Z. Shu, Passive vehicle suspensions employing inerters with multiple performance requirements, Journal of Sound and Vibration, 2014.
[11] F. Scheibe, M.C. Smith, Analytical solutions for optimal ride comfort and tyre grip for passive vehicle suspensions, Vehicle System Dynamics, 2009.
[12] M.C. Smith, S.J. Swift,Design of passive vehicle suspensions for maximal least damping ratio, Vehicle System Dynamics, 2016.
[13] S. Evangelou, D.J.N. Limebeer, RS. Sharp, MC. Smith, Mechanical steering compensation for high-performance motorcycles. Journal of Applied Mechanics, 2007.
[14] F.C. Wang, M.K. Liao, B.H. Liao, W.J. Su, H.A. Chan, The performance improvements of train suspension systems with mechanical networks employing inerters, Vehicle System Dynamics, 2009.
[15] J.Z. Jiang, A.Z. Matamoros-Sanchez, R.M. Goodall, M.C. Smith, Passive suspensions incorporating inerters for railway vehicles. Vehicle System Dynamics, 2011.
[16] I.F. Lazar, S. Neild, D. Wagg, Using an inerter-based device for structural vibration suppression. Earthquake Engineering and Structural Dynamics, 2014.
[17] S.Y. Zhang, J.Z. Jiang, S. Neild, Optimal configurations for a linear vibration suppression device in a multi-storey building, Structural Control and Health Monitoring, 2016.
[18] Y. Li, J.Z. Jiang, S. Neild, Inerter-based configurations for main landing gear shimmy suppression. Journal of Aircraft, 2016.
[19] R. Bott, R.J. Duffin, Impedance synthesis without use of transformers. Journal of Applied Physics, 1949.
[20] S.Y. Zhang, J.Z. Jiang, S. Neild, Passive vibration control: a structure-immittance approach, Proceedings of the Royal Society, part A, 2017.
[21] M.M.S. Kaldas, K. Caliskan, R. Henze, F. Kucukay, Optimization of damper top mount characteristics to improve vehicle ride comfort and harshness, Shock and Vibration, 2014.
[22] A.N. Thite, F Coleman, M. Doody, N. Fisher, Experimentally validated dynamic results of a relaxation-type quarter car suspension with an adjustable damper, Journal of low frequency noise, vibration ans active control, 2017.
[23] L. Zuo, S.A. Nayfeh, Structures H2 optimisation of vehicle suspensions based on multi-wheel models, VSD, 2003.
[24] B. HeiBing and M. Ersoy, Chassis Handbook, Vieweg Teubner Verlag, Springer Fachmedien Wiesbaden GmbH, 1st edition, 2011.
[25] K. Wolff, R. Kraaijeveld, J. Hoppermans. Objective evaluation of subjective driving impressions. JSAE, Spring Meeting; 2008 May 21; Yokohama, Japan.
[26] P. Zandbergen, A.G. Consolaro, Ford motor companys new real suspension architecture for the global CD plateform, Proceedings of the FISITA 2012 World automotive congress.
[27] X.F. Liu, J.Z. Jiang, B. Titurus, A. Harrison, Model identification methodology for fluid-based inerters, Mechanical Systems and Signal Processing, 2018.
[28] X.Q. Sun, Y.F. Cai, L. Chen, Y.L. Liu, S.H. Wang, Vehicle height and posture control of

the electronic air suspension system using the hybrid system approach, Vehicle System Dynamics, 2016.
[29] H.G.D. Goyder, R.G. White, Vibration power flow from machines into built up structures, Journal of Sound and Vibration, 1980.
[30] M. Fraggstedt, Vibrations, Damping and power dissipation in car tyres. Doctoral Thesis, KTH Royal Institute of Technology, 2008.